LIMNOLOGY and OCEANOGRAPHY

ASLO

Limnol. Oceanogr. 69, 2024, 1247–1259

doi: 10.1002/lno.12567

Amino acid carbon isotope profiles provide insight into lability and origins of particulate organic matter

Peihong Kang,[1] Lingyu Ma,[1] Han Zhang,[2] Xi Dai,[1] Jie Liu,[1] Weifang Chen,[1] Tiantian Tang [1,3*]

[1]State Key Laboratory of Marine Environmental Science, College of Ocean and Earth Sciences, Xiamen University, Xiamen, Fujian, China

[2]Key Laboratory of Urban Environment and Health, Institute of Urban Environment, Chinese Academy of Sciences, Xiamen, Fujian, China

[3]Xiamen Key Laboratory of Urban Sea Ecological Conservation and Restoration (USER), Xiamen, Fujian, China

Abstract

Identifying the phytoplankton origin of particulate organic matter (POM) in the deep ocean is challenging due to the changing phytoplankton composition and varied extent of decomposition by heterotrophic bacteria and zooplankton. Here, we report vertical distributions of amino acid stable carbon isotope values ($\delta^{13}C$) measured in particles in the South China Sea. Carbon-weighted amino acid $\delta^{13}C$ values generally parallel bulk POM $\delta^{13}C$ profiles with a positive offset from 2.4‰ in the surface water to 6.0‰ in deep. Accordingly, a lability model is introduced to describe the relative distribution and isotopic linkage of labile and refractory particulate organic carbon. Temporal changes of amino acid $\delta^{13}C$ were observed during the microbial decomposition of two phytoplankton strains, the prokaryote cyanobacterium *Synechococcus* and the eukaryote diatom *Thalassiosira weissflogii*. Principal component analysis of individual amino acid $\delta^{13}C$ values from the decomposing cells separate samples into two components, reflecting the influence of microbial decomposition and taxonomic differences, respectively. These two components were further applied to particles. A major contribution from decomposing phytoplankton to particles below the euphotic zone was observed, with more prokaryote organic matter in the basin and a larger contribution from eukaryotes at stations near the productive northern shelf. Our findings show the applicability of amino acid $\delta^{13}C$ values in tracing the lability and phytoplankton origins of POM in samples with varied extents of decomposition in marine environments.

One of the few natural ways that CO_2 is removed from the atmosphere is through export by sinking particles that originated from primary production in the euphotic zone. In contrast, most suspended particles are generally considered to be rapidly decomposed and recycled in the upper ocean. However, Boyd et al. (2019) suggest that both suspended and sinking particles can be injected into the deep ocean through multiple pathways, and that sinking particles alone are only part of the carbon transport budget (Boyd et al. 2019). In either case, the ability of particles to be exported is largely determined by their phytoplankton origins. Large phytoplankton with biomineral structures reach the sediments due to better protection of organic matter by the associated biominerals (Engel et al. 2009) and thus higher setting velocity in the water column (Buesseler 1998; Armstrong et al. 2002). However, smaller prokaryotic phytoplankton may also be exported into the deep ocean. Such smaller "packages" of phytoplankton organic matter unassociated with minerals are frequently observed in the deep sea and may be packaged and exported from surface waters as fecal pellets or through aggregation/disaggregation processes (Close et al. 2013). Certain cyanobacterial strains can incorporate Si and Mg minerals, thus aiding the export of cyanobacterial organic matter (Tang et al. 2014). Therefore, a better understanding of the origin of both suspended and sinking particles in the deep ocean will allow a more reliable prediction of the ocean carbon budget, an important need considering how phytoplankton compositions in surface waters shift under the stress of climate change (Fu et al. 2016; Laufkötter et al. 2016).

A new approach to identify phytoplankton origins of organic matter in marine ecosystems is through the use of compound-specific carbon isotope analysis of amino acids (McCarthy et al. 2004; Close 2019). This technique is based on

*Correspondence: tiantian.tang@xmu.edu.cn

Additional Supporting Information may be found in the online version of this article.

Author Contribution Statement: P.K. analyzed the field data and wrote the manuscript. L.M. conducted the incubation experiment. H.Z. set up the method and analyzed the data. X.D. measured the POC. J.L. and W.C. deployed the pump and collected particle samples. T.T. designed the research, organized the idea, and wrote the manuscript.

the characteristic carbon isotope fractionation that occurs during the biosynthesis of major groups of organisms (Hayes 2001; Larsen et al. 2009). Essential amino acids like leucine and isoleucine can be transferred across food chains with no fractionation, which is thought to be due to the absence of pathways to synthesize essential amino acids and to the resulting obligate uptake of these amino acids from the food source (O'Brien et al. 2002). This has allowed the broad application of amino acid $\delta^{13}C$ values to trace carbon sources in a variety of ecosystems. For example, amino acid $\delta^{13}C$ values were applied to identify the origins of sediment organic matter produced by microalgae, large algae, higher plants, or bacteria (Larsen et al. 2013, 2015). They have even been used to differentiate the metabolic patterns in a strain of sulfur-oxidizing bacteria, *Allochromatium vinosum*, grown either photoautotrophically or photoheterotrophically (Tang et al. 2017). In deep-water corals, amino acid $\delta^{13}C$ time series can record historical changes in phytoplankton communities between cyanobacteria and eukaryote phytoplankton (McMahon et al. 2015; Shen et al. 2021). Amino acid isotopic signatures of exported particulate organic matter (POM) in the subtropical gyre of the Pacific have been used to identify the carbon and nitrogen transfer from POM to zooplankton (Hannides et al. 2013).

Most deep-water POM originates from the surface primary production, pinpointing the exact phytoplankton origin of those phytodetritus can be challenging, as decomposition may not only remineralize the organic matter into CO_2, but can also modify its molecular composition (Wakeham and Lee 2019). These modifications are especially extensive for more labile components like amino acids, resulting in a preferential decomposition of amino acids during particle export in the water column. A critical question that must be addressed before amino acid $\delta^{13}C$ values can reliably be used to trace the source of marine particles is how decomposition can modify the amino acid isotope fingerprinting of POM. We will begin to address this question by comparing amino acid carbon isotope fingerprinting during experimental decomposition of representative phytoplankton species with those measured in particles from the South China Sea.

The characteristic environment of the South China Sea makes this region an excellent place to evaluate the relative contributions of prokaryotic and eukaryotic phytoplankton to deep-water POM. The South China Sea is a typical oligotrophic subtropical region with characteristic seasonal variations in phytoplankton composition: prokaryotic phytoplankton dominate the phytoplankton community in the summer due to the strong stratification in the surface water and limited supply of nutrients, while winter monsoons result in upwelling nutrients, thus larger eukaryotes dominate in the winter (Ning et al. 2005; Xiao et al. 2018). Particle export in the basin responds to seasonal changes in phytoplankton composition on the surface partially due to eddy injection (Zhou et al. 2013; Cai et al. 2015), suggesting the influence of phytoplankton composition to carbon cycling in this region. Both diatoms and cyanobacteria are major components in the phytoplankton community of oligotrophic water in subtropical areas with their relative abundance varying depending on seasons, water depth, and distance from the coasts (Xiao et al. 2018).

The purpose of this work is to identify the phytoplankton origins of POM that is being transported into the deep ocean. This will provide critical support for the argument that selective export of POM from different phytoplankton taxa results in uncertainties in the ocean carbon budget, which, in turn, may meet the deep ocean microbial carbon demand. Selective export should be better evaluated for the prediction of future ocean carbon cycling due to the shift of the phytoplankton community as a response to climate change.

Materials and methods

Particle collection

Samples were collected from the R/V *Tan Kah Kee* in June of 2018 in the northeast of South China Sea and the Luzon Strait. Particles were sampled throughout the 3500-m water column at Stas. A19 (South East Asian Time-series [SEATs]), B03, and G3 (Fig. 1). Using an in situ Filtration System (McLane), around 1000 L of water from each depth was pumped through 0.7 μm pre-combusted glass-fiber filters (GF/F). This sampling approach provides somewhat comparable POM distributions to those collected by small-volume filtration (Liu et al. 2005). All filters were kept frozen at −20°C for later analysis of bulk organic carbon and amino acids. Concentrations of chlorophyll *a* were extracted with 90% acetone and measured via fluorometry (Turner Designs Model 10) (Parsons et al. 1984). Dissolved phosphate,

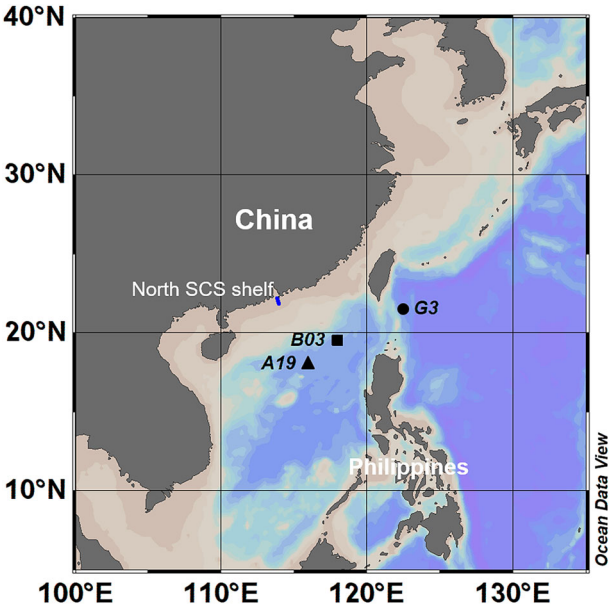

Fig. 1. Location of sampling sites in South China Sea (SCS) in July 2018. Figure was produced using Ocean Data View (version 5.1.7).

nitrate, and nitrite and silicate concentrations were measured on board following the methods of Han et al. (2012).

Degradation incubations

During the cruises in June of 2018 and May of 2020, we conducted shipboard incubations with two phytoplankton species, the cyanobacteria *Cyanobacterium Synechococcus* sp. CCMP1334 and the diatom *Thalassiosira weissflogii* CCMP102. Briefly, the phytoplankton cells were first grown axenically in an L1 medium prepared with 0.2 μm-filtered, aged surface seawater from the South China Sea basin. The algae were harvested at the end of the exponential growth stage or early stationary stage by centrifugation, and the cell pellets were frozen until use. The pellets were resuspended into 0.2 μm filtered surface seawater and inoculated with unfiltered surface seawater with its natural microbial community. The inoculated cultures were incubated in the dark at 20°C for 30 d for cyanobacteria and 47 d for diatoms. Subsamples were collected on pre-combusted glass-fiber filters, which were stored at −20°C before analysis. The diatom subsamples were collected after 0, 3, 8, 15, 32, and 47 d, and the cyanobacteria subsamples were collected after 0, 3, 6, 10, 16, and 30 d. Incubation details are described in Supporting Information Methods.

Bulk organic carbon concentrations and $\delta^{13}C$ values

Total organic carbon contents and $\delta^{13}C$ values of particulate organic carbon (POC) were analyzed using the methods of Kao et al. (2012). An area of 176.6 mm^2 was removed from the in situ pump GFF filters. For deep particles, two or three subfilters were combined. The filters were acidified with several drops of 37% HCl, dried overnight at 60°C to remove inorganic carbon, and then packed into tin capsules, $\delta^{13}C$ ratios relative to a VPDB standard were measured by an elemental analyzer (EA)-isotope ratio mass spectrometer (IRMS; Isoprime 500). Acetanilide (Merck; −27.34‰) and glutamic acid (USGS-40; −26.24‰) were used to monitor and calibrate the carbon concentrations and isotope values. The relative analytical standard deviation of bulk carbon concentration was 0.25%, and the standard deviation of carbon isotope values was 0.5‰.

Compound-specific isotope analysis of amino acids

Individual amino acid $\delta^{13}C$ ratios of particles were measured following the method of Silfer et al. (1991) as modified by Kang et al. (2021). Subsamples of around 0.2 mg organic carbon were punched from 142-mm filters of each sample. The subsamples, together with internal standard norleucine (NLeu), were hydrolyzed in 6 mol L^{-1} HCl (trace-metal clean; Sigma-Aldrich) for 20 h at 110°C to release amino acids. The dried samples were resuspended in 1 mol L^{-1} HCl for purification with Dowex 50 W × 8 cation exchange chromatography (Takano et al. 2010). Before analysis, purified amino acid fractions were derivatized with acidified isopropanol (20% acetyl chloride) and trifluoroacetic anhydride (25% CH_2Cl_2). Derivatives of 11 amino acids, alanine (Ala), glycine (Gly), valine (Val), leucine (Leu), isoleucine (Ile), proline (Pro), aspartic acid (Asp), glutamic acid (Glu), phenylalanine (Phe), lysine (Lys), and tyrosine (Tyr), were separated, and the $\delta^{13}C$ values of individual amino acids were measured via gas chromatography (GC, 60 m × 0.25 mm, 0.25 μm, HP-5MS)—combustion—IRMS (Thermo Delta V Advantage) as previously described. In parallel to the samples, a mixture of amino acid standards (Sigma-Aldrich) and NLeu with known $\delta^{13}C$ values were derivatized and analyzed as external standards. $\delta^{13}C$ values of individual amino acids standards were calibrated by EA-IRMS. Triplicate injections of external standards were used to calibrate the $\delta^{13}C$ values of individual amino acids from the derived carbon for the samples analyzed on the same day (Silfer et al. 1991). The $\delta^{13}C$ values (‰) of individual amino acids were reported relative to a VPDB standard. The linearity and drifting of isotope values were monitored by mixed *n*-alkane isotope standard B5 (Indiana University) and reference CO_2 before and after runs. The standard deviations of amino acid $\delta^{13}C$ values were calculated from the result of triplicate analysis of each sample derivative, resulting in standard deviations of carbon-weighted amino acid $\delta^{13}C$ (*w*AA $\delta^{13}C$) ranging from 0.1‰ to 1.5‰. The concentrations and molecular composition of amino acids (mol%) were quantified using the peak areas of samples and standards as well as the internal standards. The $\delta^{13}C$ values of the total hydrolyzable amino acids were expressed as the carbon-weighted mean of amino acid $\delta^{13}C$ values as in Eq. 1:

$$w\text{AA } \delta^{13}C = \sum \left(\text{AA}_i\ \delta^{13}C \times \text{AA}_i\ \text{Cmol\%}\right), \quad (1)$$

where *w*AA $\delta^{13}C$ is the sum of all individual amino acid $\delta^{13}C$ values (AA_i $\delta^{13}C$) multiplied by their relative carbon molar concentrations (AA_i C mol%). Essential and non-essential amino acid $\delta^{13}C$ profiles and leucine-normalized amino acid $\delta^{13}C$ values were compared for culture samples (Supporting Information Figs. S1, S2) and field samples (Supporting Information Figs. S5–S8) separately.

Principal component analysis and other statistical analysis

Principal component analysis was applied to amino acid $\delta^{13}C$ values normalized relative to leucine $\delta^{13}C$ that were obtained from subsamples of the degradation incubations. The factor coefficients of the first two principal components identified from degradation incubations were further used to obtain the site scores of particles as in Eq. 2, in which the scores are the sum of the normalized individual amino acid $\delta^{13}C$ values of particles multiplied by the factor coefficients (fac $coef_i$) of each amino acid in the first or second component:

$$\text{Site scores} = \sum \left(\frac{\text{normAA}_i\ \delta^{13}C - \text{AVGAA}_i\ \delta^{13}C}{\text{SDAA}_i\ \delta^{13}C} \times \text{fac coef}_i\right), \quad (2)$$

where *i* is the individual amino acid; $normAA_i$ $\delta^{13}C$ is the individual amino acid $\delta^{13}C$ of particles normalized relative to

leucine $\delta^{13}C$; and $AVGAA_i$ and $SDAA_i$ are the mean value and standard deviation of this amino acid $\delta^{13}C$ from the incubation samples. Analysis of first-order degradation rate constants of cell degradation, Bayesian mixing model for amino acid $\delta^{13}C$ values, degradation index from relative amino acid concentrations, and linear discriminant analysis of essential amino acid $\delta^{13}C$ are described in the Supporting Information Methods.

Construction of lability model

To explain the processes regulating isotopic distributions of amino acids and bulk POC in the water column, a theoretical model is introduced for particles in the ocean based on the following assumptions:

It is assumed that POC in the ocean is composed of labile organic carbon (LOC) and refractory organic carbon (ROC), both of which are assumed to originate from phytoplankton in the surface water. LOC is assumed to have the same isotope values as *w*AA $\delta^{13}C$ observed in this study. The $\delta^{13}C$ of LOC and ROC may vary across the water column, but the isotopic difference between LOC and ROC is assumed to remain constant as it reflects the characteristic metabolic pathway of phytoplankton cells to synthesize those molecules. Thus, the refractory $\delta^{13}C$ values have a constant offset, Δ, from the *w*AA $\delta^{13}C$ as in Eq. 3. During the transport of POC from the surface to the deep-water column, decomposition decreases the relative abundance of labile fraction in POC (%LOC), and correspondingly increases the relative abundance of refractory fraction (%ROC). Decomposition is assumed to have a negligible effect on the isotope ratios of either LOC or ROC. Based on mass and isotopic balance, the vertical molecular and isotopic distribution of the two fractions can be described by Eqs. 4, 5, from which the POC $\delta^{13}C$ values are determined by the relative abundance and the isotopic values of the two fractions as in Eq. 6.

$$\delta^{13}C_{ROC} = \delta^{13}C_{LOC} + \Delta^{13}C_{LOC-ROC}, \quad (3)$$

$$[POC] = [LOC] + [ROC], \quad (4)$$

$$\delta^{13}C_{POC} \times [POC] = \delta^{13}C_{LOC} \times [LOC] + \delta^{13}C_{ROC} \times [ROC], \quad (5)$$

$$\delta^{13}C_{POC} = \delta^{13}C_{LOC} + \Delta^{13}C_{LOC-ROC} \times (1 - \%LOC). \quad (6)$$

Results

Distributions of bulk POC and amino acid $\delta^{13}C$ ratios in degradation incubations

In both of our diatom and cyanobacterial incubations, POC and amino acid concentrations decreased exponentially (Fig. 2a,b; Supporting Information Figs. S1, S2). During the degradation of diatoms, the concentrations of POC and amino acid decreased after 47 d from 967 to 307 μmol C L^{-1}, and from 189 to 109 μmol C L^{-1}, respectively. Similarly, in the cyanobacterial incubation, POC and amino acid concentrations decreased after 30 d from 621 to 33 μmol C L^{-1}, and from 151 to 4 μmol C L^{-1}. The first-order degradation rate constants of POC and amino acids were larger for the cyanobacteria (0.097 and 0.124 d^{-1}) than for the diatoms (0.019 and −0.004 d^{-1}).

During the diatom degradation incubations, POC $\delta^{13}C$ values remained relatively constant from −23.8‰ to −23.0‰ (Fig. 2c,d). In contrast, POC $\delta^{13}C$ decreased in the cyanobacterial incubation from −13.4‰ to −17.3‰. Values of diatom *w*AA $\delta^{13}C$ varied over a relatively larger range, from -21.5 ± 0.7‰ to -20.8 ± 0.4‰, than POC $\delta^{13}C$ without a significant offset by the end of degradation. In the cyanobacterial incubations, *w*AA $\delta^{13}C$ increased slightly from -16.1 ± 0.3‰ to -14.2 ± 0.6‰ in contrast to the rapid decrease of POC $\delta^{13}C$. Most individual amino acids had similar $\delta^{13}C$ distributions and normalized $\delta^{13}C$ distributions relative to leucine during the diatom degradation (Fig. 2e,f; Supporting Information Figs. S1, S2; Supporting Information Table S1). But in the cyanobacterial experiment, Leu and Ile $\delta^{13}C$ varied in narrow ranges with standard deviations of 1.8‰ and 1.1‰, while Gly experienced a rapid increase with a standard deviation of up to 6.2‰ after 30 d of incubation. After 15 d, both incubations appeared to approach relatively constant concentrations and $\delta^{13}C$ values.

Distribution of bulk POC and amino acid concentrations in basin particles

During our survey in June 2018, a strong stratification in the surface water was observed with a constant depletion of nutrients in the euphotic zone (Fig. 1; Supporting Information Fig. S3a–c) and with low chlorophyll concentrations that ranged from 0.15 to 0.59 μg L^{-1} (Supporting Information Fig. S3d). Relatively deep chlorophyll maxima depths of around 65–100 m were observed. Chlorophyll concentrations at the maximal depth were lower at A19 than at the other two stations.

Organic carbon concentrations in particles ranged from 0.20 to 1.91 μmol C L^{-1} at the three stations studied (Fig. 3a). These POC concentrations were in the same range as Liu et al. (2007*b*) found in the upper 200 m at the SEATs time series in the basin. POC concentrations generally decreased with depth, with a subsurface maximum around 60–125 m, the depth at which the chlorophyll maximum was observed (Supporting Information Fig. S3d). The total amino acid concentrations of all 11 amino acids analyzed ranged from 233.06 ± 2.56 to 564.52 ± 22.31 nmol C L^{-1} in the euphotic zone, then they decreased rapidly with depth, and only about 4.57 ± 0.06 nmol C L^{-1} were found at 3000 m (Fig. 3b). At Sta. B03, the amino acid concentrations were somewhat higher than those at the other two stations. The carbon yield of amino acids relative to POC decreased from 36.8% to 2.2% over 3000 m sampled (Fig. 3c).

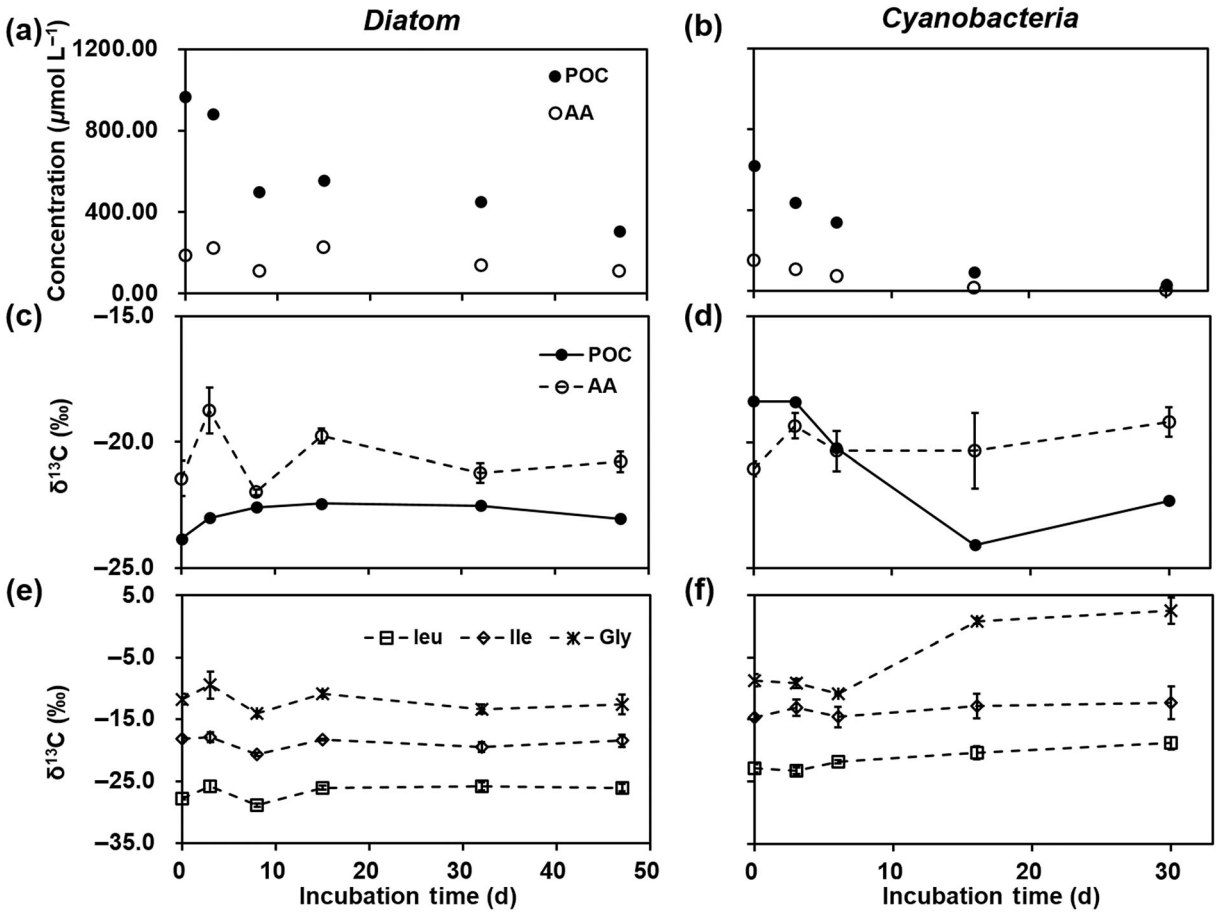

Fig. 2. The concentrations of bulk particulate organic carbon (solid symbols) and amino acids (open symbols) in diatom (**a**) and cyanobacterial (**b**) degradation incubations. The stable carbon isotope values of bulk particulate organic carbon (**c**, **d**), amino acids (*w*AA $\delta^{13}C$, **c**, **d**), and leucine (square), isoleucine (diamond) and glycine (star, **e**, **f**) in diatom (**c**, **e**) and cyanobacterial (**d**, **f**) incubations.

Distributions of bulk POC and amino acid $\delta^{13}C$ ratios in basin particles

Bulk POC $\delta^{13}C$ values in these three stations similarly ranged, from −25.7‰ to −22.3‰ (Fig. 3d). POC $\delta^{13}C$ values showed a small decrease with a depth of up to 3.4‰ as well as a subsurface minimum near the depth of the chlorophyll maximum. The distribution of POC $\delta^{13}C$ is consistent with values previously reported for particles in open ocean waters (Liu et al. 2007*b*; Close et al. 2014).

Individual amino acid $\delta^{13}C$ values from these stations ranged from -33.7 ± 0.6‰ to 15.2 ± 6.1‰ (Fig. 4; Supporting Information Figs. S4, S5). The most negative $\delta^{13}C$ values of Ala, Gly, Leu, Pro, and Phe appeared near the bottom of the euphotic zone at around 100 m (Fig. 4; Supporting Information Fig. S4). Some amino acids, usually essential ones (sensu O'Brien et al. 2002), changed little with depth below 200 m, such as Ile of -20.6 ± 0.9‰, Leu of -25.1 ± 0.6‰, and Pro of -15.3 ± 1.4‰ (Supporting Information Fig. S4). In contrast, non-essential amino acids like Val and Gly showed larger variations of -20.5 ± 4.5‰ and 0.0 ± 10.6‰, respectively (Supporting Information Fig. S5). Gly showed much higher $\delta^{13}C$ values (9.8 ± 7.6‰) at 1000, 2000, and 3000 m at A19 than those other two stations (-9.4 ± 1.6‰ and -5.7 ± 1.4‰). This difference between essential and non-essential amino acid $\delta^{13}C$ can also be observed in leucine-normalized amino acid $\delta^{13}C$ profiles (Supporting Information Figs. S6, S7). The carbon-weighted means (*w*AA $\delta^{13}C$) of amino acid $\delta^{13}C$ values ranged from -21.2 ± 0.2‰ to -17.5 ± 0.8‰. The most negative *w*AA$\delta^{13}C$ ratios were found at the depth where the chlorophyll maximum was observed. Little variation in *w*AA $\delta^{13}C$ values was observed below the euphotic zone (Fig. 3d).

Discussion

Decomposition of prokaryotic and eukaryotic phytoplankton

Our shipboard microbial degradation incubation experiments do not perfectly reflect the natural decomposition of POM in the deep water, which also includes effects from zooplankton grazing, aggregation and disaggregation, as well as mineral association. For this reason, shipboard experiments

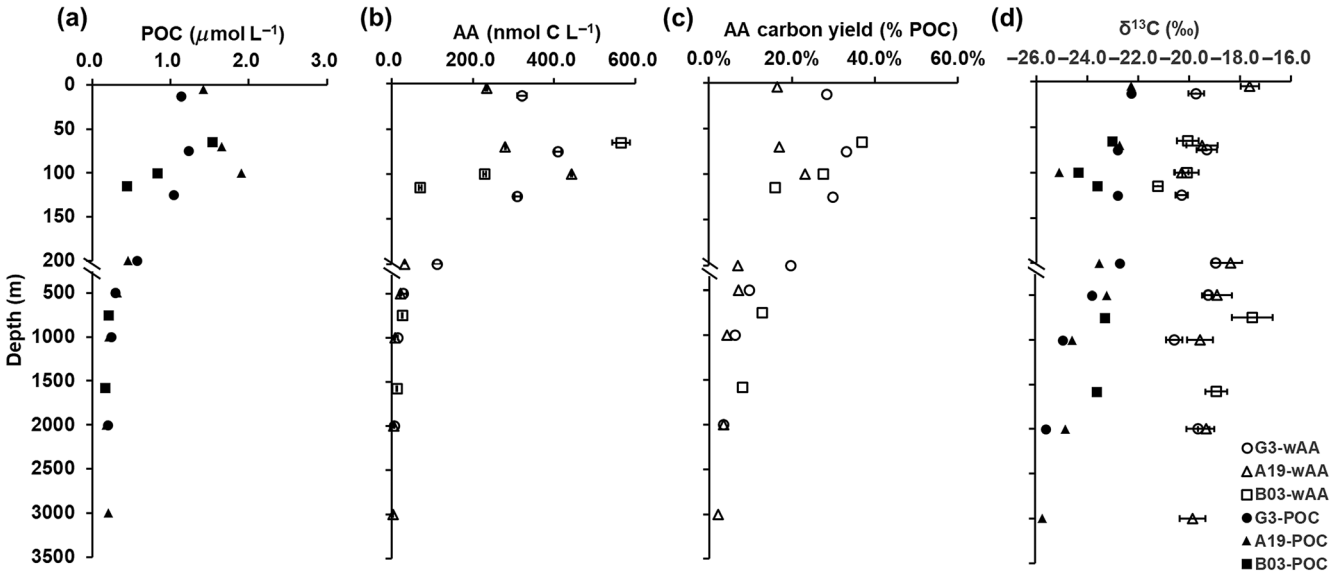

Fig. 3. The vertical distribution of (**a**) bulk particulate organic carbon, (**b**) amino acid concentrations, (**c**) the relative carbon concentrations of amino acid to POC (AA carbon yield), and (**d**) the stable carbon isotope ratios of bulk particulate organic carbon (POC $\delta^{13}C$; solid symbols) and carbon-weighted amino acids (*w*AA $\delta^{13}C$; open symbols) at G3 (circle), A19 (triangle), and B03 (square) in July 2018.

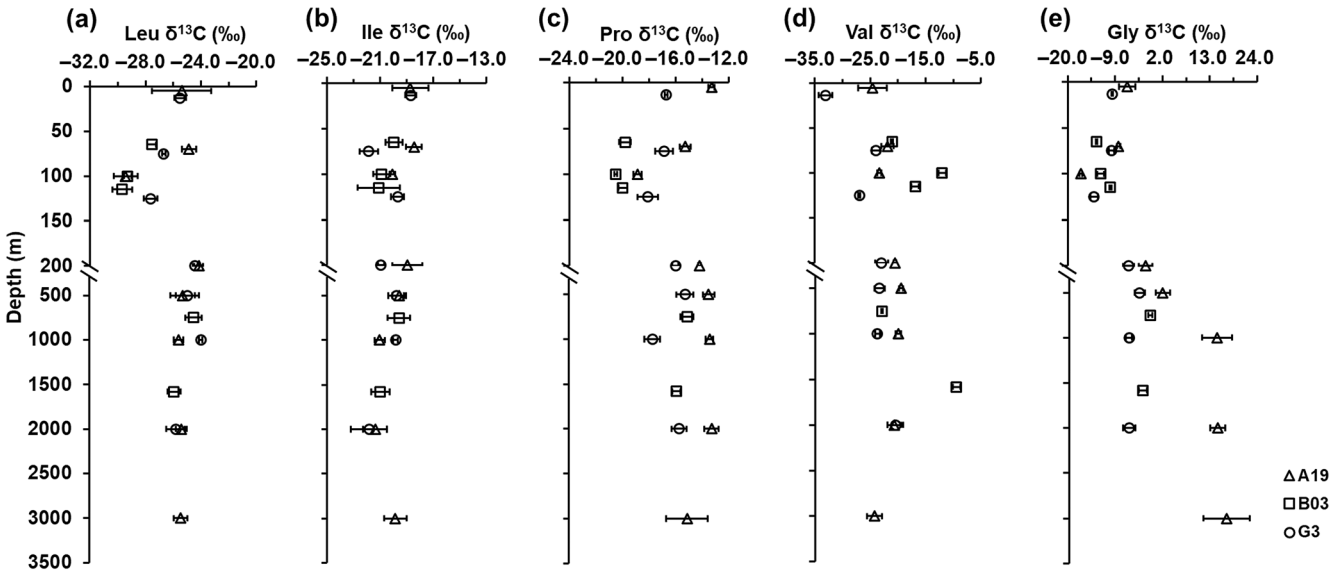

Fig. 4. The vertical distribution of individual amino acid $\delta^{13}C$ of suspended particles in South China Sea, leucine (**a**), isoleucine (**b**), proline (**c**), glycine (**d**), and valine (**e**) at G3 (circle), A19 (triangle), and B03 (square).

can only reflect the microbial degradation regulated by heterotrophic bacteria from oligotrophic subtropical surface waters. This type of degradation experimental design has been used in a number of previous studies with diatoms (e.g., Moriceau et al. 2009) and Synechococcus (e.g., Harvey et al. 1995).

During the degradation experiments, the POC degradation rate constant observed for the cyanobacteria (0.097 d^{-1}) was larger than for the diatoms (0.019 d^{-1}). These rate constants agree well with previous observations in degradation experiments using diatoms (0.025–0.082 d^{-1}; Moriceau et al. 2009) and cyanobacteria (0.025–0.129 d^{-1}; Harvey et al. 1995). Slower degradation in diatoms might result from physical protection by the silicate frustules (Abramson et al. 2009). Degradation rate constants of amino acids were generally consistent with the bulk POC, indicating that the bioavailability of individual compounds may not be a major factor determining the degradation rate of phytoplankton cellular material, but rather that protection by biominerals or

other cell membrane structures are more important in determining the degradation rates (Abramson et al. 2009).

The microbial decomposition of organic matter includes a series of diagenetic steps including, for example, cell lysis (Tang and Lee 2016), peptide hydrolysis and diffusion (Arnosti 2011), as well as uptake by heterotrophic bacteria (Mulholland and Lee 2009). A combination of all these steps likely results in the different $\delta^{13}C$ distributions of individual amino acids and POC between the two incubations. It has been reported that the $\delta^{13}C$ of glycine can increase during peptide hydrolysis (Silfer et al. 1992). This may explain the higher glycine $\delta^{13}C$ observed in cyanobacteria incubations. The increase in glycine $\delta^{13}C$ was less significant in decomposed diatoms, most likely due to the protection of cellular materials by associated biominerals. Overall the different temporal patterns in isotopic distribution observed between the two incubations reflect the difference between diatom and cyanobacteria in terms of the lability of their cellular components to microbial decomposition.

The degradation incubation shows evidence that though influenced by decompositional modification, amino acid $\delta^{13}C$ can still trace the phytoplankton origins of organic matter. In a principal component analysis of incubation samples, the first two components explain 68.8% of the relative variation in individual amino acid $\delta^{13}C$ (Fig. 5a; Supporting Information Table S5). The first component separates the fresh samples (in the first 10 d) from the more decomposed samples (after 10 d of degradation), indicating that decompositional modification is the primary regulator of the amino acid $\delta^{13}C$ variation of the incubation samples. The second component clusters the samples from diatom away from those from cyanobacteria, suggesting that the amino acid $\delta^{13}C$ difference between diatom and cyanobacterial organic matter can still be seen even after 47 d of microbial decomposition.

In the degradation incubations, the decomposed organic matter is a combination of bacterial biomass and phytoplankton debris after selective decomposition by heterotrophic bacteria. Though heterotrophic bacteria are major players in determining the isotopic composition of amino acid $\delta^{13}C$ values in POM, it is difficult to distinguish the amino acids produced by bacterial de novo synthesis from those produced by selective decomposition. This is because bacterial synthesis also records the isotopic signature of their food source, originally the organic matter photosynthesized by phytoplankton in the surface ocean. The degradation incubation suggests that the amino acid $\delta^{13}C$ signature of the original phytoplankton biomass remains even after a 30-d decomposition. This similarity in amino acid $\delta^{13}C$ is shared not only with the leftover POM from phytoplankton, but also with the POM that became a bacterial cellular substitute. This information is recorded by principal component 2. Bacterial uptake also causes a deviation of amino acid $\delta^{13}C$ distribution from the original phytoplankton species, which is recorded in principal component 1 together with the modification during the bacterial de novo synthesis. Thus, instead of evaluating the specific

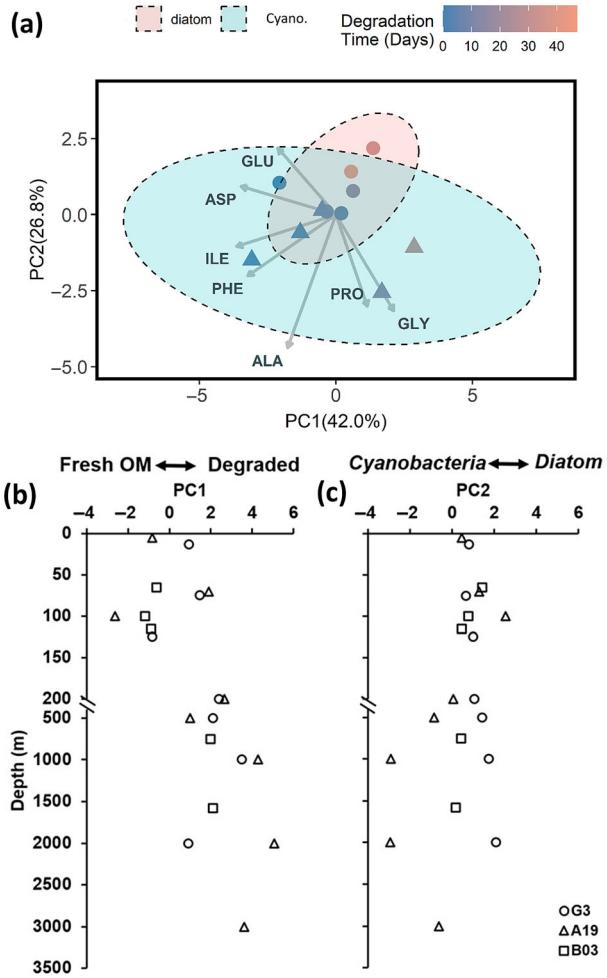

Fig. 5. The first two principal components, the first component (PC1) and the second component (PC2) (**a**), of leucine-normalized individual amino acid $\delta^{13}C$ values of subsamples from the degradation incubations of diatoms (circles) and cyanobacteria (triangle); The vertical distribution of the site scores of particles in the first component (**b**) and second component (**c**), which were calculated using the factor coefficients obtained from the principal component analysis of degradation incubation.

contribution of heterotrophic bacteria in POM, the principal component analysis here provides an alternative glimpse into the overall influence of heterotrophic bacteria on amino acid $\delta^{13}C$ distribution by recording the decomposition and origin information separately.

Isotope profiles of labile and refractory POM

Directly after production, POM is subject to extensive alteration through microbial reworking, zooplankton grazing, mineral association, and aggregation and disaggregation. Much of this alteration occurs in the upper water column and causes the molecular and isotopic composition of POM to shift from its phytoplankton origin. Amino acids are subject to more rapid decomposition than the bulk of POM (Wakeham et al. 1997). Exponential decreases in amino acid

concentrations with depth were observed in the water column and resulted in a decrease in the relative abundance of amino acids in the bulk POC (Fig. 2). Similar relative decreases have been regularly observed for labile components of POM (Wakeham and Lee 2019), which suggests a progressive shift in molecular composition from labile organic matter dominated to refractory organic matter dominated with depth (Fig. 6a).

Across the water column, *w*AA $\delta^{13}C$ generally paralleled bulk POC $\delta^{13}C$ profiles with little change of *w*AA $\delta^{13}C$ but a slight depletion in ^{13}C of POC, resulting in a positive offset between 2.4‰ and 6.0‰. This less varied *w*AA $\delta^{13}C$, assumed as the constant LOC $\delta^{13}C$ in the lability model (Fig. 6), is possible because labile component like amino acids can be more rapidly removed from the particles by remineralization. More complete removal of amino acids results in *w*AA $\delta^{13}C$ values closer to those newly supplied from the upper water, but with less influence from decompositional modification. While bulk POC is more possibly regulated by the shift in molecular composition as well as the intrinsic isotopic difference among major classes of organic compounds. The depletion of ^{13}C in POC with depth may result from the increasing contribution of isotopically negative ROC in deep water.

It needs to be clarified that amino acids are not the only class of organic compounds in LOC. Fatty acids, pigment, and certain carbohydrates can also be rapidly removed from the bulk POC. In this study, amino acids were applied as a representative of LOC because they account for a major component in the cellular content of phytoplankton and surface particles. Other labile compounds would share similar changes in relative abundance to amino acids in the water column. Intrinsic $\delta^{13}C$ differences may also exist between amino acids and other labile compounds. They should have parallel $\delta^{13}C$ distribution in vertical profiles as they share the same origin and similar geochemical behavior. Thus, the $\delta^{13}C$ of absolute "LOC" may deviate from the *w*AA$\delta^{13}C$, but the trend and relationship with bulk POC should be similar as explained by the lability model.

LOC accounts for less than 12.9% of POC in the deep water over 750 m. Consequently, the POC $\delta^{13}C$ values are approximately equal to the $\delta^{13}C$ of ROC in these deep-water particles (Fig. 7). Thus the *w*AA $\delta^{13}C$ and POC $\delta^{13}C$ of deep-water particles should follow the relationship between labile and refractory $\delta^{13}C$ as in Eq. 3. This is supported by the observed linear relationship between *w*AA $\delta^{13}C$ and POC $\delta^{13}C$ of deep-water particles, where the regression slope (slope = 1.011) is close to the presumed relationship of 1 as in Eq. 3. The regression offset further suggests that the Δ in Eq. 3 should be around −5.277‰. This offset is consistent with the previous prediction of -4.53 ± 0.48‰ ($n = 14$) for the $\delta^{13}C$ difference between the acid-soluble component of POC (dominated by amino acids) and the acid non-soluble component (dominated by ROC) in the open ocean (Hwang and Druffel 2003, 2006), indicating that a universal isotopic offset between labile and refractory molecules may exist globally in deep-water particles.

For the particles from surface and mid-depth water, the POC $\delta^{13}C$ values are determined by the relative abundance

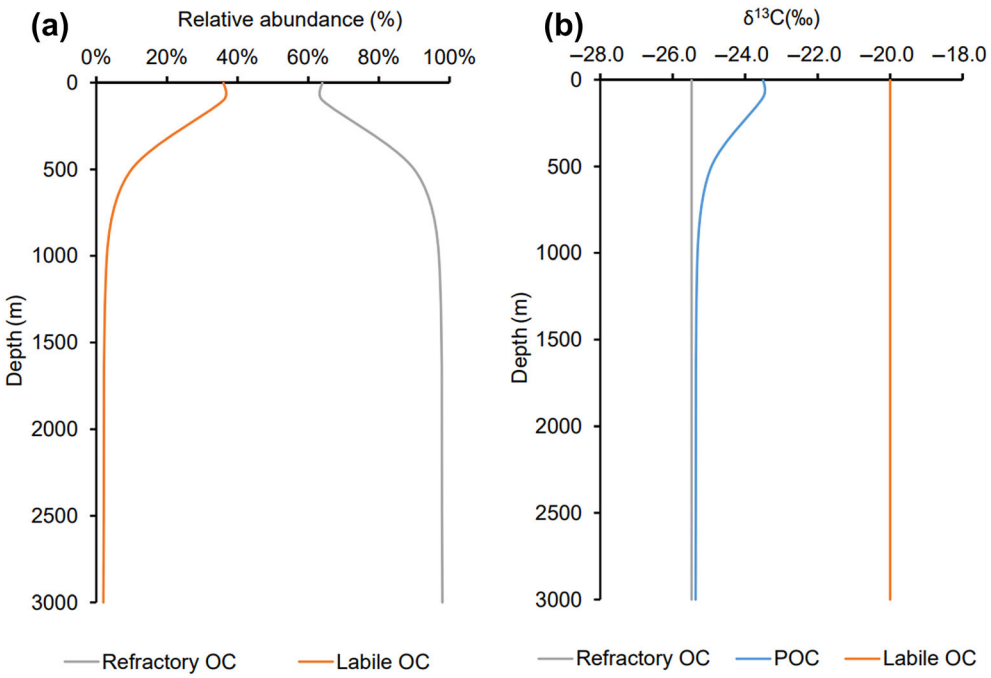

Fig. 6. Schematic diagrams of (**a**) presumed relative abundance of labile organic carbon as amino acids and refractory organic carbon in bulk POC across water column; (**b**) presumed carbon isotope values ($\delta^{13}C$) of labile, refractory, and bulk POC across water column as predicted by the lability model.

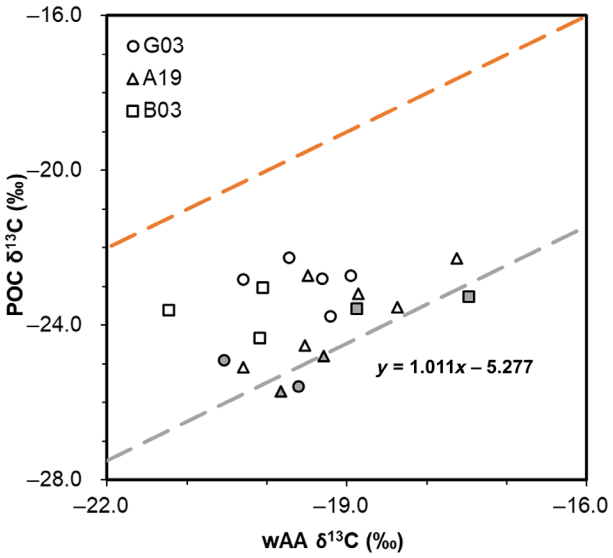

Fig. 7. Relationship between bulk particulate organic carbon $\delta^{13}C$ distribution and carbon-weighted amino acid $\delta^{13}C$ (*w*AA $\delta^{13}C$) from South China Sea basin. The linear regression for particles from deep water (> 1000 m, shapes filled in gray) is shown as the gray dashed line. The one to one line (orange dashed line) of *w*AA $\delta^{13}C$ represents an ideal condition with amino acids constituting the entire bulk organic carbon.

and the isotopic values of LOC and ROC as explained in Eq. 6. Higher abundance of LOC from upper waters results in more isotopically positive POC than in the deep-water particles which have less LOC (Fig. 7). This would explain previous observations of a negative isotopic shift in bulk POM during decomposition (Jeffrey et al. 1983: Nakatsuka et al. 1997). The lability model suggests that particles from the basin are characterized by (1) a distinctive isotopic offset between LOC and ROC, (2) the rapid decrease of the relative abundance of LOC in the upper water column, and (3) the same origin of LOC and ROC in the surface waters. The model emphasizes the distinct behaviors of LOC and ROC in particles, which largely regulate the molecular and isotopic distribution of POC during the transport of particles across the water column.

Response of individual amino acids $\delta^{13}C$ profiles to decomposition

The $\delta^{13}C$ distribution of most individual amino acids in the particles show consistent variation across the water column as observed in previous studies (Supporting Information Figs. S4–S7). Less variate $\delta^{13}C$ values across the water column were also observed in fatty acids (Close et al. 2013). Among the amino acids studied, Leu and Ile show the smallest variation in $\delta^{13}C$ values, while Gly shows progressive enrichment in ^{13}C with depth (Fig. 3). The different responses of Leu and Ile vs. Gly agree with the observed isotopic trends in our decomposing phytoplankton incubations (Fig. 2e,f). Moreover, the ^{13}C enrichment of Gly in deep-water particles varied among the three stations. The Gly $\delta^{13}C$ at A19 was somewhat higher than at B03 and G03. To better understand the influence of decomposition and phytoplankton composition on the amino acid $\delta^{13}C$ distribution in the basin, we applied the first two factor coefficients from the degradation incubations to obtain the site scores of basin particles (Fig. 5b,c; Supporting Information Table S5). Scores of particles in the first component were lowest at the bottom of the euphotic zone, where the highest chlorophyll concentrations were observed. The site scores progressively increased down the water column below the euphotic zone, indicating an increasing contribution of decomposed phytoplankton cellular material to particles in the deep-water column.

Differences were also observed in the first component scores among the three stations: deep particles at A19 were slightly higher than at B03 and G03, implying that the deep-water particles at A19 have a higher degradation state than at the other two stations. This spatial variation suggests that the deep-water particles experienced varied decompositional modifications due to the difference in phytoplankton composition (Lomas and Moran 2011), aggregation/disaggregation (Volkman and Tanoue 2002), and/or mineral association during the POM export in the water column (Ingalls et al. 2003). Among the three stations, spatial variations in phytoplankton composition (discussed in the next section) may be a major reason for the varied degradation state among stations. For example, as identified from the second principal component (Fig. 5c), more prokaryotic phytoplankton contribute to a higher degradation state of deep-water particles at the center of the basin (A19), while more efficient export of larger eukaryotic phytoplankton may contribute to the lower degradation state of particles at B3 and G03 (Cai et al. 2015; Xiao et al. 2018).

Contribution of prokaryotic and eukaryotic phytoplankton to POM

As shown in the degradation incubations, the second principal component reflected the amino acid isotopic difference between the diatoms and cyanobacteria (Fig. 5c); we can use this offset to differentiate the phytoplankton origins of POM. The site scores of particles on the second component ranged from −3 to 3. This range agrees with the observations in decomposed cyanobacterial and diatom cells (Fig. 5a). Below the euphotic zone, scores at A19 were more negative than at B03 and G03. The varied trends among the three stations suggest a greater cyanobacterial contribution to deep-water particles at A19, but a greater diatom contribution at B03 and G03.

Cyanobacteria and diatoms are major constituents of the phytoplankton community in both the South China Sea and other oligotrophic region like subtropical gyres (Liu et al. 2007*a*; Xiao et al. 2018). The two species are distinct

from each other in morphology, carbon fixation pattern and biomineral composition, which results in characteristic amino acid isotope differences between each other (McCarthy et al. 2004; Larsen et al. 2013). This difference has been applied to identify shifts in the phytoplankton community (McMahon et al. 2015). In the South China Sea, the composition of phytoplankton is highly dynamic as a response to the monsoon-driven stratification and nutrient inputs from the adjacent shelf. This may result in the larger contribution of diatom organic matter at B03 and G03, which are closer to the northern shelf and to the track of eddy intrusion from the west Pacific. Eddy subduction and lateral transport from the adjacent productive slope can enhance particle export due to a higher contribution of diatom organic matter at those two stations (Zhou et al. 2013; Shen et al. 2020). In contrast, cyanobacterial organic matter might be expected to contribute more in the center of the oligotrophic basin (A19). Our work suggests the presence of a dynamic contribution from various species of phytoplankton to deep-water POM, and supports the widely-held assumption that the amino acid $\delta^{13}C$ distribution of deep-water POM can record the variation of phytoplankton composition in the surface water, even though extensive decomposition occurs during the transport of particles in the water column (Shen et al. 2021).

Implications of labile POM geochemical behavior in the oceans

Two analyses (principal component analysis and lability model) were applied in this work, addressing different perspectives. The principal component analysis explored the relative variations in $\delta^{13}C$ among individual amino acids, which were determined by the diverse metabolic processes involved during the synthesis of those amino acids. This nature of amino acid $\delta^{13}C$ is primarily determined by the phytoplankton or bacterial metabolism, but usually independent from the "absolute" $\delta^{13}C$ values of bulk carbon, which gives the $\delta^{13}C$ baseline of individual amino acids. The lability model compares the $\delta^{13}C$ values of total amino acids with other compounds in POM, which is primarily determined by the $\delta^{13}C$ values of their shared inorganic carbon origin, the intrinsic $\delta^{13}C$ differences among major classes of organic molecules as well as their relative abundance in bulk POC.

The application of amino acid $\delta^{13}C$ as a new biomarker to characterize the decomposition and phytoplankton origins of marine particles has the following advantages. (1) Evaluating POM origins using this technique can exclude potential interference from decomposition by extracting the first two principal components from the amino acid $\delta^{13}C$ distribution as indicators of decomposition and phytoplankton origins separately; (2) the first and second components identified here use the relative variations among individual amino acid $\delta^{13}C$ values, thus filtering out the interference from the fluctuation in $\delta^{13}C$ values or molecular composition of carbon source. This, in turn, makes the two components more robust for solely tracking the degradation and phytoplankton origins; (3) this application derives from the isotopic distribution of a major cellular component, the amino acids. This avoids the potential bias using species-specific biomarkers that can show different geochemical behaviors from the major constituents of organic carbon. Nevertheless, these two indices were derived from the simulated decomposition of only two phytoplankton species, thus potential limitations are expected accordingly. The origin identification may fail in characterizing the isotopic signature of phytoplankton species other than diatom and cyanobacteria. This may provide misleading source information, particularly in the regions where diatom or cyanobacteria as the miner component of the phytoplankton community. Moreover, chemoautotrophic production or other processes may also influence the vertical distribution of amino acid $\delta^{13}C$, the contribution of which cannot be identified by this application.

Our observations of amino acid $\delta^{13}C$ patterns in marine particles provide a new approach, the lability model, to predict the lability of marine particles based on their molecular composition and compound-specific isotopic distribution. The vertical profiles of LOC and ROC can be quantified in the water column. This finding gives us a better understanding of the geochemical behavior of marine particles, demonstrating that marine particles are highly heterogeneous in origin and degradation state as a result of changing phytoplankton composition and primary production in the surface waters as well as episodic inputs of shelf organic matter by eddy subduction or lateral transport.

Data availability statement

The data that supports the findings of this study are available in the Supporting Information Material of this article.

References

Abramson, L., S. Wirick, C. Lee, C. Jacobsen, and J. A. Brandes. 2009. The use of soft X-ray spectromicroscopy to investigate the distribution and composition of organic matter in a diatom frustule and a biomimetic analog. Deep-Sea Res. II: Top. Stud. Oceanogr. **56**: 1369–1380. doi:10.1016/j.dsr2.2008.11.031

Armstrong, R. A., C. Lee, J. I. Hedges, S. Honjo, and S. G. Wakeham. 2002. A new, mechanistic model for organic carbon fluxes in the ocean based on the quantitative association of POC with ballast minerals. Deep-Sea Res. II: Top. Stud. Oceanogr. **49**: 219–236. doi:10.1016/S0967-0645(01)00101-1

Arnosti, C. 2011. Microbial extracellular enzymes and the marine carbon cycle. Annu. Rev. Mar. Sci. **3**: 401–425. doi:10.1146/annurev-marine-120709-142731

Boyd, P. W., H. Claustre, M. Levy, D. A. Siegel, and T. Weber. 2019. Multi-faceted particle pumps drive carbon sequestration in the ocean. Nature **568**: 327–335. doi:10.1038/s41586-019-1098-2

Buesseler, K. O. 1998. The decoupling of production and particulate export in the surface as a tracer of upper ocean comparisons between production and. Glob. Biogeochem. Cycles **12**: 297–310. doi:10.1029/97GB03366

Cai, P., D. Zhao, L. Wang, B. Huang, and M. Dai. 2015. Role of particle stock and phytoplankton community structure in regulating particulate organic carbon export in a large marginal sea. J. Geophys. Res.: Oceans **120**: 2063–2095. doi:10.1002/2014JC010432

Close, H. G. 2019. Compound-specific isotope geochemistry in the ocean. Annu. Rev. Mar. Sci. **11**: 27–56. doi:10.1146/annurev-marine-121916-063634

Close, H. G., S. G. Wakeham, and A. Pearson. 2014. Lipid and ^{13}C signatures of submicron and suspended particulate organic matter in the Eastern Tropical North Pacific: Implications for the contribution of bacteria. Deep-Sea Res. I: Oceanogr. Res. Pap. **85**: 15–34. doi:10.1016/j.dsr.2013.11.005

Close, H. G., and others. 2013. Export of submicron particulate organic matter to mesopelagic depth in an oligotrophic gyre. Proc. Natl. Acad. Sci. USA **110**: 12565–12570. doi:10.1073/pnas.1217514110

Engel, A., L. Abramson, J. Szlosek, Z. Liu, G. Stewart, D. Hirschberg, and C. Lee. 2009. Investigating the effect of ballasting by $CaCO_3$ in *Emiliania huxleyi*, II: Decomposition of particulate organic matter. Deep-Sea Res. II: Top. Stud. Oceanogr. **56**: 1408–1419. doi:10.1016/j.dsr2.2008.11.028

Fu, W., J. T. Randerson, and J. Keith Moore. 2016. Climate change impacts on net primary production (NPP) and export production (EP) regulated by increasing stratification and phytoplankton community structure in the CMIP5 models. Biogeosciences **13**: 5151–5170. doi:10.5194/bg-13-5151-2016

Han, A., M. Dai, S. Kao, J. Gan, Q. Li, L. Wang, and W. Zhai. 2012. Nutrient dynamics and biological consumption in a large continental shelf system under the influence of both a river plume and coastal upwelling. Limnol. Oceanogr. **57**: 486–502. doi:10.4319/lo.2012.57.2.0486

Hannides, C. C. S., B. N. Popp, C. Anela Choy, and J. C. Drazen. 2013. Midwater zooplankton and suspended particle dynamics in the North Pacific Subtropical Gyre: A stable isotope perspective. Limnol. Oceanogr. **58**: 1931–1936. doi:10.4319/lo.2013.58.6.1931

Harvey, H. R., J. H. Tuttle, and J. T. Bell. 1995. Kinetics of phytoplankton decay during simulated sedimentation: Changes in biochemical composition and microbial activity under oxic and anoxic conditions. Geochim. Cosmochim. Acta **59**: 3367–3377. doi:10.1016/0016-7037(95)00217-N

Hayes, J. M. 2001. Fractionation of carbon and hydrogen isotopes in biosynthetic processes. Rev. Mineral. Geochem. **43**: 225–277. doi:10.2138/gsrmg.43.1.225

Hwang, J., and E. R. M. Druffel. 2003. Lipid-like material as the source of the uncharacterized organic carbon in the ocean? Science **299**: 881–884. doi:10.1126/science.1078508

Hwang, J., and E. R. M. Druffel. 2006. Carbon isotope ratios of organic compound fractions in oceanic suspended particles. Geophys. Res. Lett. **33**: L23610. doi:10.1029/2006GL027928

Ingalls, A. E., C. Lee, S. G. Wakeham, and J. I. Hedges. 2003. The role of biominerals in the sinking flux and preservation of amino acids in the Southern Ocean along 170°W. Deep-Sea Res. II: Top. Stud. Oceanogr. **50**: 713–738. doi:10.1016/S0967-0645(02)00592-1

Jeffrey, A. W. A., R. C. Pflaum, J. M. Brooks, and W. M. Sackett. 1983. Vertical trends in particulate organic carbon ^{13}C: ^{12}C ratios in the upper water column. Deep-Sea Res. I: Oceanogr. Res. Pap. **30**: 971–983. doi:10.1016/0198-0149(83)90052-3

Kang, P., H. Zhang, Z. Yang, Y. Zhu, B. He, and T. Tang. 2021. A model of algal organic carbon distributions in the Pearl River estuary using the amino acid carbon isotope values. Geochim. Cosmochim. Acta **294**: 1–12. doi:10.1016/j.gca.2020.11.010

Kao, S. J., J.-Y. Terence Yang, K. K. Liu, M. Dai, W. C. Chou, H. L. Lin, and H. Ren. 2012. Isotope constraints on particulate nitrogen source and dynamics in the upper water column of the oligotrophic South China Sea. Glob. Biogeochem. Cycles **26**: GB2033. doi:10.1029/2011GB004091

Larsen, T., D. L. Taylor, M. B. Leigh, and D. M. O'Brien. 2009. Stable isotope fingerprinting: A novel method for identifying plant, fungal, or bacterial origins of amino acids. Ecology **90**: 3526–3535. doi:10.1890/08-1695.1

Larsen, T., M. Ventura, N. Andersen, D. M. O'Brien, U. Piatkowski, and M. D. McCarthy. 2013. Tracing carbon sources through aquatic and terrestrial food webs using amino acid stable isotope fingerprinting. PloS One **8**: e73441. doi:10.1371/journal.pone.0073441

Larsen, T., L. T. Bach, R. Salvatteci, Y. V. Wang, N. Andersen, M. Ventura, and M. D. McCarthy. 2015. Assessing the potential of amino acid ^{13}C patterns as a carbon source tracer in marine sediments: Effects of algal growth conditions and sedimentary diagenesis. Biogeosciences **12**: 4979–4992. doi:10.5194/bg-12-4979-2015

Laufkötter, C., and others. 2016. Projected decreases in future marine export production: The role of the carbon flux through the upper ocean ecosystem. Biogeosciences **13**: 4023–4047. doi:10.5194/bg-13-4023-2016

Liu, H., J. Chang, C. M. Tseng, L. S. Wen, and K. K. Liu. 2007*a*. Seasonal variability of picoplankton in the Northern South China Sea at the SEATS station. Deep-Sea. Res. II:

Top. Stud. Oceanogr. **54**: 1602–1616. doi:10.1016/j.dsr2.2007.05.004

Liu, K. K., S. J. Kao, H. C. Hu, W. C. Chou, G. W. Hung, and C. M. Tseng. 2007*b*. Carbon isotopic composition of suspended and sinking particulate organic matter in the northern South China Sea—From production to deposition. Deep-Sea. Res. II: Top. Stud. Oceanogr. **54**: 1504–1527. doi:10.1016/j.dsr2.2007.05.010

Liu, Z., and others. 2005. Why do POC concentrations measured using Niskin bottle collections sometimes differ from those using in-situ pumps? Deep-Sea Res. I: Oceanogr. Res. Pap. **52**: 1324–1344. doi:10.1016/j.dsr.2005.02.005

Lomas, M. W., and S. B. Moran. 2011. Evidence for aggregation and export of cyanobacteria and nano-eukaryotes from the Sargasso Sea euphotic zone. Biogeosciences **8**: 203–216. doi:10.5194/bg-8-203-2011

McCarthy, M. D., R. Benner, C. Lee, J. I. Hedges, and M. L. Fogel. 2004. Amino acid carbon isotopic fractionation patterns in oceanic dissolved organic matter: An unaltered photoautotrophic source for dissolved organic nitrogen in the ocean? Mar. Chem. **92**: 123–134. doi:10.1016/j.marchem.2004.06.021

McMahon, K. W., M. D. McCarthy, O. A. Sherwood, T. Larsen, and T. P. Guilderson. 2015. Millennial-scale plankton regime shifts in the subtropical North Pacific Ocean. Science **350**: 1530–1533. doi:10.1126/science.aaa9942

Moriceau, B., and others. 2009. Si–C interactions during degradation of the diatom *Skeletonema marinoi*. Deep-Sea Res. II: Top. Stud. Oceanogr. **56**: 1381–1395. doi:10.1016/j.dsr2.2008.11.026

Mulholland, M. R., and C. Lee. 2009. Peptide hydrolysis and the uptake of dipeptides by phytoplankton. Limnol. Oceanogr. **54**: 856–868. doi:10.4319/lo.2009.54.3.0856

Nakatsuka, T., N. Handa, N. Harada, T. Sugimoto, and S. Imaizumi. 1997. Origin and decomposition of sinking particulate organic matter in the deep water column inferred from the vertical distributions of its $\delta^{15}N$, δ^{13} and δ^{14}. Deep-Sea Res. I: Oceanogr. Res. Pap. **44**: 1957–1979. doi:10.1016/S0967-0637(97)00051-4

Ning, X., F. Chai, H. Xue, Y. Cai, C. Liu, and J. Shi. 2005. Physical-biological oceanographic coupling influencing phytoplankton and primary production in the South China Sea. J. Geophys. Res.: Oceans **109**: C10005. doi:10.1029/2004JC002365

O'Brien, D. M., M. L. Fogel, and C. L. Boggs. 2002. Renewable and nonrenewable resources: Amino acid turnover and allocation to reproduction in Lepidoptera. Proc. Natl. Acad. Sci. USA **99**: 4413–4418. doi:10.1073/pnas.072346699

Parsons, T. R., Y. Maita, and C. M. Lalli. 1984. A manual of chemical and biological methods for seawater analysis. Pergamon Press. doi:10.1016/C2009-0-07774-5

Shen, Y., T. P. Guilderson, O. A. Sherwood, C. G. Castro, F. P. Chavez, and M. D. McCarthy. 2021. Amino acid $\delta^{13}C$ and $\delta^{15}N$ patterns from sediment trap time series and deep-sea corals: Implications for biogeochemical and ecological reconstructions in paleoarchives. Geochim. Cosmochim. Acta **297**: 288–307. doi:10.1016/j.gca.2020.12.012

Shen, J., and others. 2020. Laterally transported particles from margins serve as a major carbon and energy source for dark ocean ecosystems. Geophys. Res. Lett. **47**: e2020GL088971. doi:10.1029/2020GL088971

Silfer, J. A., M. H. Engel, S. A. Macko, and E. J. Jumeau. 1991. Stable carbon isotope analysis of amino acid enantiomers by conventional isotope ratio mass spectrometry and combined gas chromatography/isotope ratio mass spectrometry. Anal. Chem. **63**: 370–374. doi:10.1021/ac00004a014

Silfer, J. A., M. H. Engel, and S. A. Macko. 1992. Kinetic fractionation of stable carbon and nitrogen isotopes during peptide bond hydrolysis: Experimental evidence and geochemical implications. Chem. Geol. **101**: 211–221. doi:10.1016/0009-2541(92)90003-N

Takano, Y., Y. Kashiyama, N. O. Ogawa, Y. Chikaraishi, and N. Ohkouchi. 2010. Isolation and desalting with cation-exchange chromatography for compound-specific nitrogen isotope analysis of amino acids: Application to biogeochemical samples. Rapid Commun. Mass Spectrom. **24**: 2317–2323. doi:10.1002/rcm.4651

Tang, T., K. Kisslinger, and C. Lee. 2014. Silicate deposition during decomposition of cyanobacteria may promote export of picophytoplankton. Nat. Commun. **5**: 4143. doi:10.1038/ncomms5143

Tang, T., and C. Lee. 2016. The role of surface layer proteins in the degradation of a photosynthetic prokaryote, the cyanobacterium *Synechococcus* sp. Mar. Chem. **186**: 33–45. doi:10.1016/j.marchem.2016.07.003

Tang, T., W. Mohr, S. R. Sattin, D. R. Rogers, P. R. Girguis, and A. Pearson. 2017. Geochemically distinct carbon isotope distributions in *Allochromatium vinosum* DSM 180^T grown photoautotrophically and photoheterotrophically. Geobiology **15**: 324–339. doi:10.1111/gbi.12221

Volkman, J. K., and E. Tanoue. 2002. Chemical and biological studies of particulate organic matter in the ocean. J. Oceanogr. **58**: 265–279. doi:10.1023/A:1015809708632

Wakeham, S. G., and C. Lee. 2019. Limits of our knowledge, part 2: Selected frontiers in marine organic biogeochemistry. Mar. Chem. **212**: 16–46. doi:10.1016/j.marchem.2019.02.005

Wakeham, S. G., C. Lee, J. I. Hedges, P. J. Hernes, and M. L. Peterson. 1997. Molecular indicators of diagenetic status in marine organic matter. Geochim. Cosmochim. Acta **61**: 5363–5369. doi:10.1016/S0016-7037(97)00312-8

Xiao, W., L. Wang, E. Laws, Y. Xie, J. Chen, X. Liu, B. Chen, and B. Huang. 2018. Realized niches explain spatial gradients in seasonal abundance of phytoplankton groups in the South China Sea. Prog. Oceanogr. **162**: 223–239. doi:10.1016/j.pocean.2018.03.008

Zhou, K., M. Dai, S. J. Kao, L. Wang, P. Xiu, F. Chai, J. Tian, and Y. Liu. 2013. Apparent enhancement of ^{234}Th-based particle export associated with anticyclonic eddies.

Earth Planet. Sci. Lett. **381**: 198–209. doi:10.1016/j.epsl.2013.07.039

Acknowledgments

We thank the reviewers for their very helpful comments. We thank X. Liu and L. F. Wang for the chlorophyll and nutrient data, J. H. Chen, L. Tian, and W.B. Zou for assistance with EA-IRMS analysis, and B. M. Liu, Y. Y. Li, and X. H. Wang for assistance with GC–MS analysis. We thank C. Lee for her comments on the manuscript. J. N. Cai, X. R. Chen, C. M. Ye, and Y. Y. Gao deployed the CTD and in situ pump. We appreciate the help of the captain and crew of R/V "*Tan Kah Kee*." This work is supported by the National Natural Science Foundation of China (Project No. 41976035 and 41703070). Samples were collected onboard R/V "*Tan Kah Kee*" during research cruise NORC2018-05, NORC2019-06, and NORC2020-06 supported by NSFC Shiptime Sharing Project (project number: 41749905, 41849906, and 41949906).

Conflict of interest statement

The authors declare no conflict of interest.

Submitted 08 March 2023
Revised 29 October 2023
Accepted 30 March 2024

Associate editor: Elizabeth Kujawinski